Functional surface reconstructions of hexagonal SiC

2004 J. Phys.: Condens. Matter 16 S1705

(http://iopscience.iop.org/0953-8984/16/17/013)

INSTITUTE OF PHYSICS PUBLISHING JOURNAL OF PHYSICS: CONDENSED MATTER

J. Phys.: Condens. Matter **16** (2004) S1705–S1720 PII: S0953-8984(04)65082-X

Functional surface reconstructions of hexagonal SiC

K Heinz[1], J Bernhardt[1], J Schardt[1] and U Starke[1,2]

[1] Lehrstuhl für Festkörperphysik, Universität Erlangen-Nürnberg, Staudtstraße 7, D-91058 Erlangen, Germany
[2] Max-Planck-Institut für Festkörperforschung, Heisenbergstraße 1, D-70569 Stuttgart, Germany

E-mail: kheinz@fkp.physik.uni-erlangen.de and Klaus.Heinz@physik.uni-erlangen.de

Received 23 June 2003
Published 16 April 2004
Online at stacks.iop.org/JPhysCM/16/S1705
DOI: 10.1088/0953-8984/16/17/013

Abstract

The basal surfaces of hexagonal SiC exhibit a large variety of surface reconstructions that develop under a similarly rich variety of sample preparations. A subset of these surface phases, which have been investigated in structural detail using scanning tunnelling microscopy and quantitative low-energy electron diffraction, is described and shown to offer the scope to be used for the formation of SiC-based semiconductor devices. The phases discussed are the (3×3) and $(\sqrt{3} \times \sqrt{3})$R30° reconstructions for the (0001) surfaces of 4H- and 6H-SiC and the oxygen-uptake-driven $(\sqrt{3} \times \sqrt{3})$R30°-$SiO_x$ reconstructions of these polytypes for both the (0001) and the $(000\bar{1})$ surface orientations. We show that the (3×3) reconstruction corresponds to a highly passivated surface that facilitates hexagonal single-crystal growth, while suitable preparation of the $(\sqrt{3} \times \sqrt{3})$R30° reconstruction favours a switch to cubic growth and hence to the formation of a heterojunction. The $(\sqrt{3} \times \sqrt{3})$R30°-$SiO_x$ reconstructions promise to form defect-free interfaces to insulating silicon oxide films, which is important for device applications.

(Some figures in this article are in colour only in the electronic version)

1. Technological importance of SiC surfaces

The exceptional properties of SiC that make it a usable semiconductor under demanding conditions are based on the material's bulk. A large electronic band gap, together with a high electron mobility and thermal conductivity, allows use at, for example, high temperatures or high power and frequency. At a first glance, the surface of the material only comes into play when electrodes need to be contacted. Yet the surface also plays an important role when the material is to be used in devices such as MOSFETs or heterojunctions, for example. In this case, a transition to an oxide or a material with a different band gap must be realized. So as not to inhibit the functioning of such devices, defects that are simultaneously built into

the interface must largely be avoided. SiC seems to be a promising candidate in this respect too, as one may naively suspect that the transition to SiO_2 should be eased by silicon being a constituent of both materials and by their lattice parameters differing by just a few per cent. Yet the SiO_2/SiC interfaces prepared so far are of very limited quality with substantial defect densities [1], i.e. much higher than those realized for SiO_2/Si. Obviously, the surface oxidation process is not controlled to the extent that defect creation is avoided. Similar features hold for the formation of heterojunctions, for which SiC appears to be ideal because of its parent polytypism: depending on the polytype, the band gap varies between 2.4 and 3.3 eV while the corresponding variation of the lattice parameter is only in the region of a 1000th so that the formation of a sharp, stress- and defect-free heterojunction should be easy. Yet this requires a controlled transition from one polytype to another during growth and, of course, this is again dominated by surface properties. Similarly, this also applies to the control of homo-polytype growth, i.e. the growth of single crystals.

Given this importance of SiC surfaces, in this review we investigate them with respect to their behaviour under various conditions such as silicon enrichment or depletion (realized during growth conditions) or exposure to hydrogen and oxygen (frequently realized during sample preparation). We will see that these conditions can lead to surface superstructures that vary from simple adatom structures to phases in which the atomic arrangement within the surface has changed (equivalent to the formation of another polytype) or, by oxygen uptake, to phases with oxidic adlayers. We hereby concentrate on the basal, i.e. (0001)-oriented surfaces of hexagonal SiC, and on the surface reconstructions that can be useful for crystal growth or device formation [2, 3]. The main techniques that can be applied to retrieve the morphology and crystallographic structure of the surface phases addressed are scanning tunnelling microscopy (STM) and low-energy electron diffraction (LEED), including the quantitative version of the latter. Additional information about stoichiometry and chemical bonding was gained from Auger electron spectroscopy (AES). Since they are standard surface sensitive tools, there is no need to describe these techniques. In the next section we first introduce the structural basic of the material then survey the sequence of the various superstructures that develop through application of certain preparation recipes.

2. Hexagonal SiC: structural basics and surface preparation

2.1. Structural basics

In principle, the atomic arrangement in SiC is similar to that in Si, since each atom is bonded tetrahedrally to its neighbours, whereby in SiC these neighbours are chemically different. The tetrahedron is shown in figure 1(a) and the lateral formation of a (111)- or (0001)-oriented SiC double-layer is displayed in panel (b). For vertical stacking, i.e. along the crystal's *c*-axis, there are two possibilities. Panel (c) depicts the *continued or linear stacking*, as indicated by the dark bonding sticks which always have the same orientation (*staggered orientation*). In contrast, the next tetrahedron can be rotated by 60°, i.e. the stacking from one to the next double layer can be switched, as indicated in figure 1(d) (*switched stacking* or *eclipsed orientation*). This degree of freedom with respect to stacking and the nearly degenerate bonding energies involved [4] are responsible for the rich polytypism of SiC [5]. When the stacking is always continued, the cubic structure (C) results, whereby translation by three double-layer spacings along the [111] direction (*c*-axis) leaves the crystal invariant (zincblende structure; also called 3C-SiC, i.e. '3 layers' and 'Cubic'). Each switch in stacking leads to a certain polytype. So, a switch every double-layer (ABAB . . . sequence), equivalent to hexagonal (H) stacking, leads to the so-called 2H (=wurtzite) structure (2 spacings with translational periodicity). With different

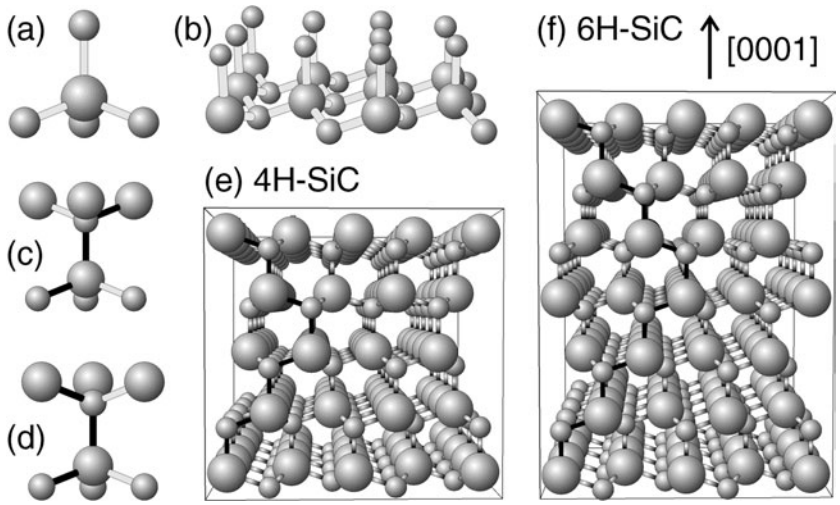

Figure 1. A tetrahedron (a), made up of one silicon and four carbon atoms (the large and small spheres, respectively). In (b) these units are assembled into an atomic layer. The orientation of tetrahedra in the next layer to be stacked can be the same (c) or rotated by 60° (d). This leads to different stacking scenarios, as displayed for the 4H and 6H structures in (e) and (f), respectively (where the stacking direction is indicated by dark bonding sticks).

linear stacking arrays in slabs separated by switches in stacking, for example the hexagonal 4H and 6H structures result, as displayed in figures 1(e) and (f), with 4 and 6 spacing translational periodicity, respectively.

In this paper we concentrate on the above-mentioned 4H and 6H polytypes, particularly since most applications of the material are for the hexagonal crystal type. Also, these surfaces are representative, in the sense that there can be different surface terminations which—due to the existence of steps—coexist on the surface in different domains, i.e. there are different stacking sequences below the surface in each domain, as indicated schematically in figure 2. While each domain exhibits three-fold rotational symmetry, the superposition of diffraction patterns of equally weighted domains rotated by 60° with respect to each other (e.g. $S3_{6H}$ and $S3^{*}_{6H}$ in figure 2) leads to a six-fold LEED pattern, as indicated schematically in the lower part of figure 2. Of course, the same scenario also holds for the 'other side' of the crystal, i.e. for a nominal C-termination of a bulk (bi-layer) truncated surface (the 'C-face'), which in the following will be denoted as $(000\bar{1})$ orientation while the notation (0001) refers to the nominal Si termination (the 'Si-face'). We emphasize that these different stacking scenarios in different surface domains do not apply to 3C surfaces with only linear stacking involved. It is interesting to see if, and how, the stacking below the surface influences the surface geometry (including reconstructions and adsorbate geometries) or how the stacking at the surface is modified, for example, by an excess of one of the constituents, by adsorbates, or by the surface preparation procedure in general.

2.2. Surface preparation

In most cases the preparation of SiC surfaces is realized in two steps, i.e. *ex situ* preparation followed by *in situ* preparation (at this point we give only a survey of the results and in the subsequent sections concentrate on the structure of the developing phases). The first step aims to obtain a crystallographically and morphologically well defined surface, as obtained

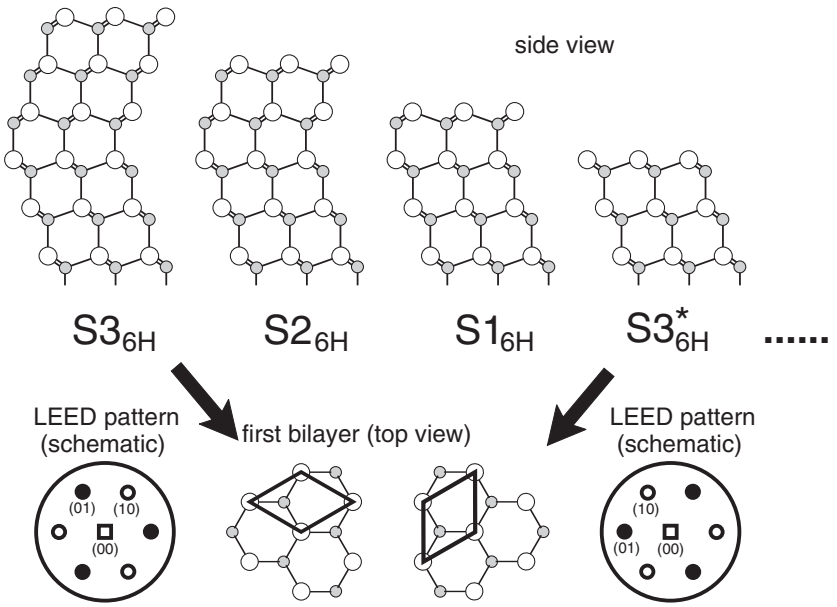

Figure 2. Top: possible stacking sequences at the surface of a 6H-SiC(0001) sample, for example. Sn indicates that there is a switch in stacking n layers below the surface. Sn* domains differ from Sn domains by a 60° rotation. Bottom: Sn and Sn* domains produce equivalent but 60°-rotated diffraction patterns, so that equal weights of such domains give rise to six-fold symmetric patterns.

for example either by exposure to hydrogen at atmospheric pressure and high temperatures or by deliberately oxidizing the surface followed by removal of the oxide by hydrofluoric acid. After introduction of the prepared samples into an ultra-high vacuum (UHV), (1×1)-periodic surfaces are observed in the latter case (see [6] for a review of (1×1)-structures). For the other *ex situ* preparation procedure, a $(\sqrt{3} \times \sqrt{3})$R30°-$SiO_x$ superstructure is found. We will show in section 5 that the latter is characterized by a silicate adlayer (different in composition for (0001) and $(000\bar{1})$ orientations). The suffix 'SiO_x' is to distinguish it from another phase of the same symmetry (see below). The $(\sqrt{3} \times \sqrt{3})$R30°-$SiO_x$ phase results only when residual oxygen is not avoided. Accordingly, a recent investigation shows that pure hydrogen treatment also results in (1×1) periodicity [7].

The second step (i.e. *in situ* preparation) can be started on both kinds of *ex situ* prepared samples. Simple annealing or annealing under additional Si deposition is used. Except for the immediately developing superstructure, the following phases are independent of the *ex situ* preparation, as indicated in figure 3 for the two surface orientations. For SiC(0001), the annealing of the *ex situ*-prepared (1×1) phase under Si-flux, i.e. by maintaining Si-rich conditions, leads to a (3×3) superstructure with intense extra spots, while on the $(000\bar{1})$ orientation a silicon-rich (2×2) superstructure develops (denoted $(2 \times 2)_{Si}$). For both surface orientations, further annealing at about 1000 °C makes the surface pass through states with coexisting metastable phases (for a description see [8]), after which further superstructures develop, as shown in figure 3.

We do not aim to present the surface structures of all the phases that appear. Instead, we concentrate on phases in which the surface has changed in a way which can possibly be used in the functional sense, as described in the introductory section, for example to facilitate single-crystal growth, form sharp heterojunctions or an almost defect-free interface to SiO_2 for surface passivation, or for use in MOSFET devices. In the following sections we first concentrate on

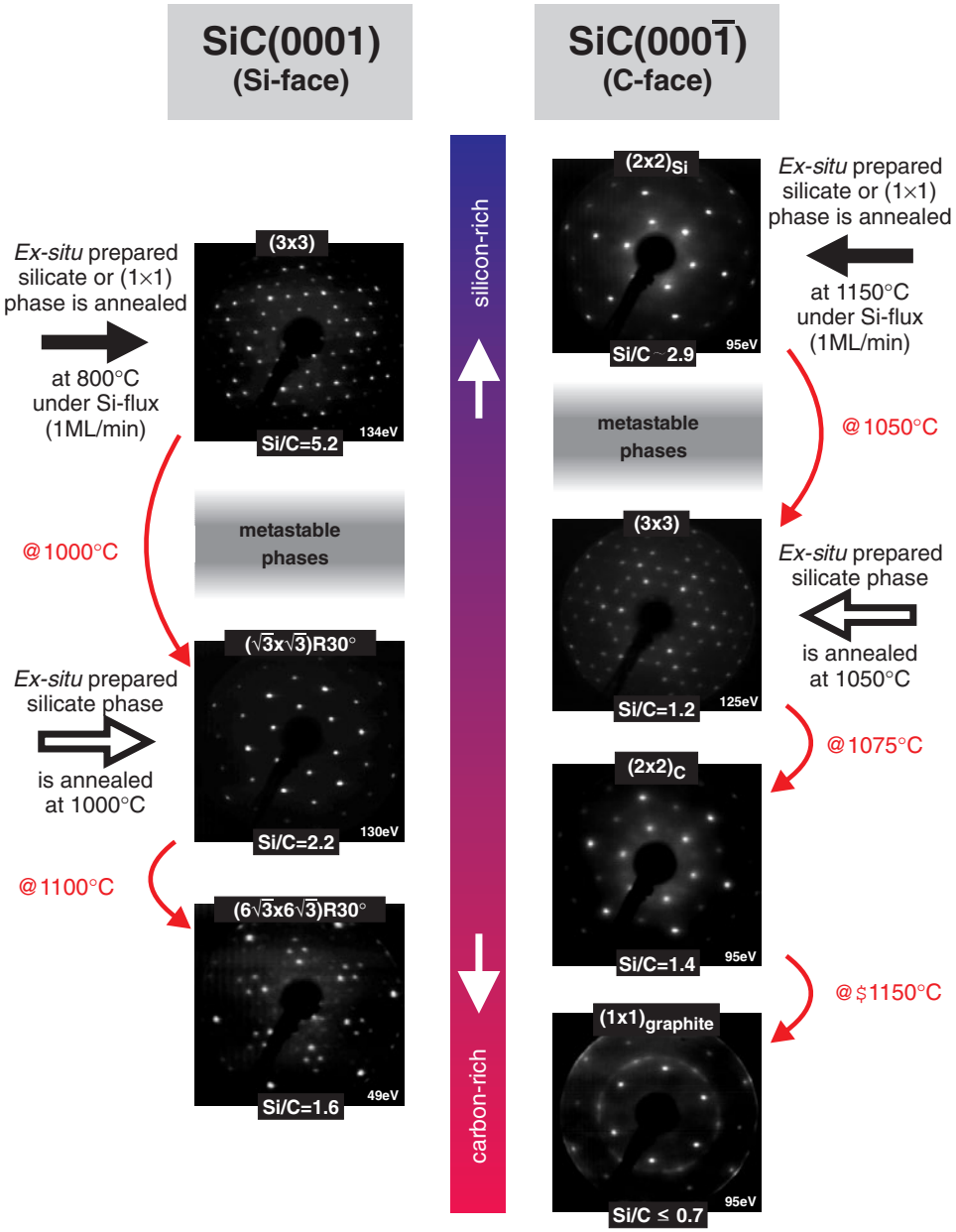

Figure 3. Superstructure phases developing from the *in situ* treatment of *ex situ*-prepared (0001)- and (000$\bar{1}$)-oriented SiC surfaces.

the *in situ*-prepared phases and, in the penultimate section, address the *ex situ*-prepared silicate phases that are observed for both surface orientations.

3. Dangling-bond minimized (3 × 3)-SiC(0001) and crystal growth

As indicated in figure 3, the *ex situ*-prepared SiC(0001) surface (both 4H and 6H polytypes) transforms into a (3 × 3) superstructure when annealed at about 800 K under simultaneous

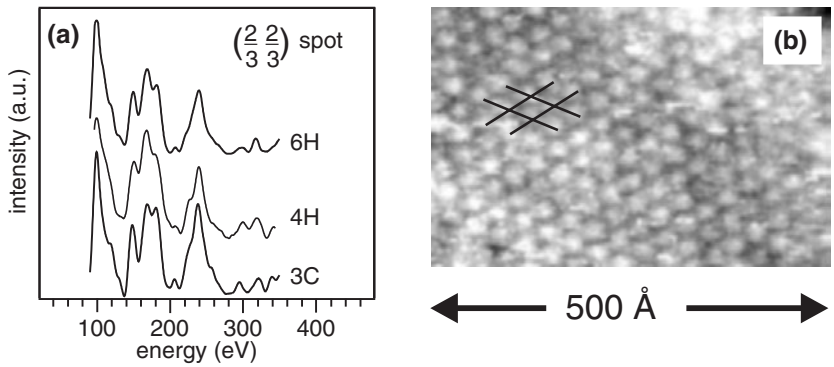

Figure 4. Left: LEED intensity spectra of a selected fractional order beam of the (3 × 3) superstructure prepared on 3C-SiC(111), 4H-SiC(0001) and 6H-SiC(0001). Right: an STM image taken for the (3 × 3) surface reconstruction of 4H-SiC(0001).

exposure to silicon flux [9]. The same superstructure also develops for a 3C-SiC(111) film grown on Si(111) [10] whereby, presumably, the extra silicon supply is provided by diffusion from the substrate. It also appears that the LEED intensity spectra are largely the same, as demonstrated in figure 4(a). This is indicative of the fact that differences in stacking—to which the spectra are very sensitive [11, 12]—are much below the surface, so that they are at most only weakly probed by the impinging electrons. Equivalently, this means that the surface must by covered by additional silicon layers formed due to the silicon flux offered. This is apparent more directly from the Auger peak-to-peak intensity ratio of Si and C [9, 13, 14] which, as shown by the labels below the LEED patterns in figure 3, is the highest for all phases that appear.

The STM images of the (3 × 3) superstructure, as shown for the 4H polytype in figure 4(b), exhibit just a single protrusion per (3 × 3) unit cell. Therefore, a surface model that was originally suggested by Kaplan [9] can be ruled out since, for that model to be a (3 × 3) analogue to the dimer–adatom-stacking-fault (DAS) reconstruction of (7 × 7)-Si(111), two adatoms per unit cell (and possibly a corner hole) should show up. A proposed modification of the DAS model with just one adatom per cell [15] or a model with simple Si tetramers arranged on the surface [16] had to be sorted out too. This was achieved by an unconventional evaluation of the LEED intensities that is based on the existence of a single surface-protruding adatom per unit cell serving as a beam splitter for the in-coming electrons, allowing a holographic-type data evaluation (for a recent review of the method, see [17]). Applied to the present case [18], it yields the immediate atomic surrounding of the beam splitter atom, as shown in figure 5. Here, panel (a) presents the image as reconstructed directly from the measured intensities and panel (b) gives the corresponding ball model for clarity. The full structure of this new type of surface reconstruction was completed and refined by using conventional quantitative LEED [14, 10, 19], which results in the model displayed in figure 5(c). Evidently, on the bulk-like terminated substrate (of which only the last SiC double-layer is displayed) there is a full adlayer of Si atoms on which Si tetramers are arranged. The stacking of these tetramers with respect to the substrate is rotated by 60°, i.e. it corresponds to a faulted orientation in the (7 × 7)-Si(111) DAS model's sense.

Details of the crystallographic structure are given in figure 6 in the top (a) and side (b) views. The surface-protruding adatom resides in a T_4 site and is the only atom in the (3 × 3) unit cell that still possesses a dangling bond. The bonds of all the other atoms are saturated,

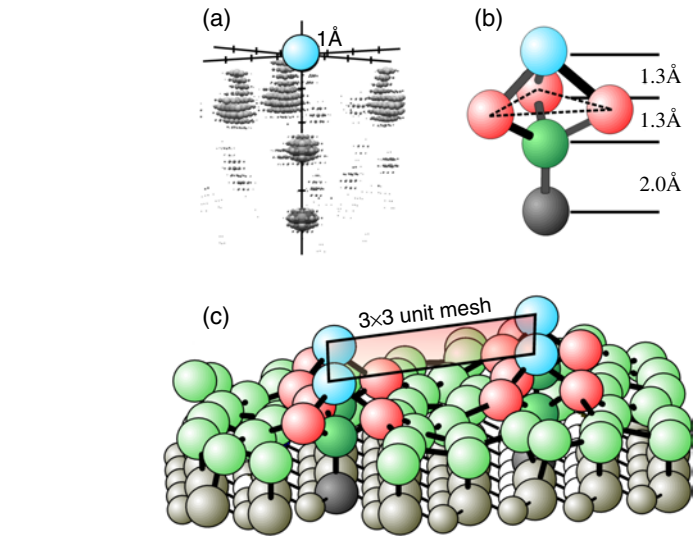

Figure 5. (a) A structural element of the (3 × 3) surface reconstruction observed on the 3C-, 4H- and 6H-SiC surfaces, as retrieved by direct holographic-type evaluation of LEED intensities, and repeated in (b) using a ball model. The adatom itself, indicated by the ball in panel (a), defines the origin of the holographic reconstruction. Panel (c) displays a ball model of the full (3 × 3) structure in perspective view. The atoms retrieved by holography are visible on the left-hand side through omission of some of the surrounding atoms.

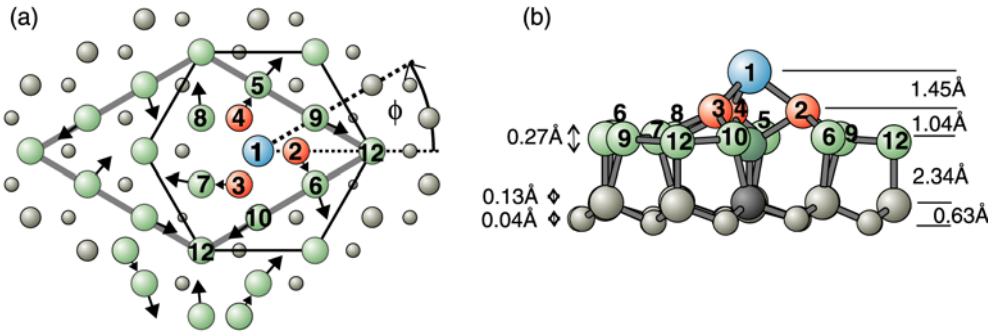

Figure 6. (a) Top and (b) side view models of the (3 × 3) surface reconstruction. On the left, some rotation ($\Delta\Phi \approx 9°$) of the atoms below the surface-protruding adatom (no 1) is illustrated. On the right, the buckling induced in the adlayer and top substrate bi-layer, together with interlayer spacings, are given. The rotation and buckling lead to an optimization of Si–Si bond lengths.

i.e. only one out of nine dangling bonds of a bulk terminated surface is left. This substantial surface passivation is accompanied by an optimization of the Si–Si bond lengths in the adlayer, which comes from some rotation of atoms around the adatom ($\Delta\Phi \approx 9°$, equivalent to lateral displacements of up to 0.74 Å) and from some layer buckling, as shown in figure 6. The final bond lengths vary only between 2.31 and 2.35 Å and hence are rather close to the ideal value (2.35 Å). The adlayer atomic orbitals are sp^2-hybridized, since the atoms are three-fold coordinated to in-plane atoms. The structure is in quantitative agreement with the results of first-principles calculations [10, 20, 21].

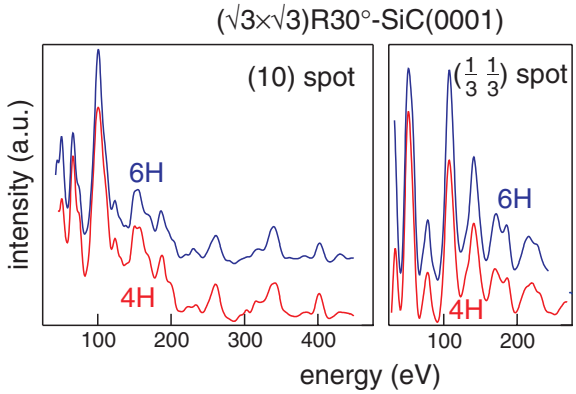

Figure 7. A comparison of LEED intensity spectra of $(\sqrt{3} \times \sqrt{3})$R30° phases on 4H- and 6H-SiC(0001) for a selected integer order spot (left) and fractional order spot (right).

The surface passivation that has been described provides a reasonable explanation of the observation that, by applying chemical vapour deposition (CVD) or molecular beam epitaxy (MBE), there is qualitatively good crystal growth under Si-rich conditions [22–24]. In particular, this is when the substrate is slightly mis-cut with respect to the basal plane. Then the surface exhibits steps, so the arriving atoms can copy the underlying polytype by diffusion to the steps, where they are attached in the crystallographically correct way [25]. Obviously, this diffusion and hence homoepitaxial growth is facilitated most when the surface is passivated, i.e. when it possesses the (3×3) reconstruction induced by Si-rich growth conditions.

4. Stacking rearrangements induced by preparing $(\sqrt{3} \times \sqrt{3})$R30°-SiC(0001)

As indicated in figure 3, annealing the above-described (3×3) phase at about 1000 °C leads to the formation of a $(\sqrt{3} \times \sqrt{3})$R30° phase. This is for both 4H- and 6H-SiC(0001), and figure 7 shows the spectra of an integer and fractional order beam for the two prepared polytype phases. Evidently, the spectra of both types of spots are almost identical, i.e. the underlying atomic structures must be equal, too. The similarity between the fractional order data means that the structural elements that are arranged to produce the superstructure are similar for the two surfaces, which can easily be realized. On the other hand, the similarity between integer order spot intensities—which are dominated by the substrate's stacking characteristics [11, 12, 19]—means that the stacking within the substrate is similar. This comes as a real surprise, because the 6H polytype differs from the 4H polytype through its additional ability to exhibit S3-stacked domains at the surface, which cannot appear on a bulk-like terminated 4H surface. We address the issues of superstructure crystallography and substrate stacking one after another in the following.

The STM reveals that there is only one surface-protruding atom in the unit cell, as shown in figure 8. The LEED analysis confirms this quantitatively [2, 26, 27], whereby the structural model displayed in figure 8 also results. The adatom resides on the T4 site (with the substrate layer atoms slightly shifted towards the adatom in the lateral direction) and induces some buckling in the first C-sublayer, as indicated. Additionally, the analysis also detected a buckling (≈0.1 Å) in the neighboured Si-sublayer in the second substrate bi-layer (not shown in the figure). The values of geometric parameters given in the figure are for the above-mentioned preparation and for the 4H polytype, but are the same for 6H-SiC within the limits of error of the

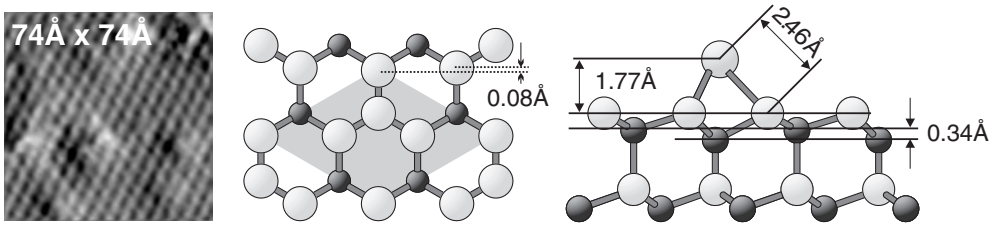

Figure 8. Left: An STM image of the $(\sqrt{3} \times \sqrt{3})$R30° reconstruction on 4H-SiC(0001). Middle and right: a ball model of the crystallographic structure of the $(\sqrt{3} \times \sqrt{3})$R30° reconstruction from top and side views, respectively.

Table 1. A comparison of weights for domains with stacking sequences S1, S2 and S3 for 6H and 4H sample surfaces, different 4H samples ((a) versus (b)) and different preparations (I, II, III) of the $(\sqrt{3} \times \sqrt{3})$R30° reconstruction on the same sample (for details, see text).

	Sample type	Preparation method	S1 (%)	S2 (%)	S3 (%)
1	6H	I: annealing (3 × 3) phase	10	0	90
2	4H (a)	I: annealing (3 × 3) phase	10	10	80
3	4H (b)	I: annealing (3 × 3) phase	20	15	65
4	4H (b)	II: annealing silicate phase	15	75	10
5	4H (b)	III: annealing under Si-flux	15	50	35

structural analyses (<0.1 Å) [8, 19, 28]. They compare favourably with results of calculations using density functional theory (DFT) [29–31]. X-ray diffraction (XRD) experiments [32] and coaxial impact-collision ion scattering spectroscopy (CAICISS) [33] also produced the T4 model, but failed to resolve the induced substrate buckling and yield considerably different bond lengths for the adatom.

While the adsorption structure retrieved is unspectacular, the stacking sequence in the substrate that was detected by quantitative LEED is surprising, as already mentioned. As shown in table 1 (lines 1 and 2), the LEED analyses reveal that the stacking sequence S3 is realized in both the 4H and 6H samples and is even the dominant domain in both cases. The result is much outside the limits of error of the analyses (of the order of ±10% for the domain weights). Obviously, by annealing the Si-rich (3 × 3) phase, an S3-stacked domain is formed (at the expense of S1- and S2-stacked areas), i.e. there is a tendency for cubic stacking (though no S4-stacked domains are found within the limits of error of the LEED analyses when these domains are allowed in the fitting procedure [8]).

While the final weights of differently stacked domains within the $(\sqrt{3} \times \sqrt{3})$R30° phase can depend to a certain extent on which sample is actually used, a drastic influence stems from the method by which the superstructure phase is prepared. So, a 4H sample nominally similar to that considered so far exhibits slightly different integer order spectra (compare curve I in figure 10 with that of the 4H sample in figure 7). The evaluation yields a smaller but still dominant S3-stacked domain (sample (b) versus (a) in table 1, lines 2 and 3). Obviously, the actual surface morphology or step distribution plays some role in the surface reorganization. However, different ways to prepare the $(\sqrt{3} \times \sqrt{3})$R30° phase—as shown in figure 9—lead to strongly different stacking weights, as indicated by the changes in the integer order spectra shown in figure 10. So, the second method for preparing the $(\sqrt{3} \times \sqrt{3})$R30° phase, i.e. by annealing the *ex situ*-prepared silicate phase (indicated in figure 9, and to be addressed below), leads to a different stacking distribution, as reflected by the modifications in spectrum II

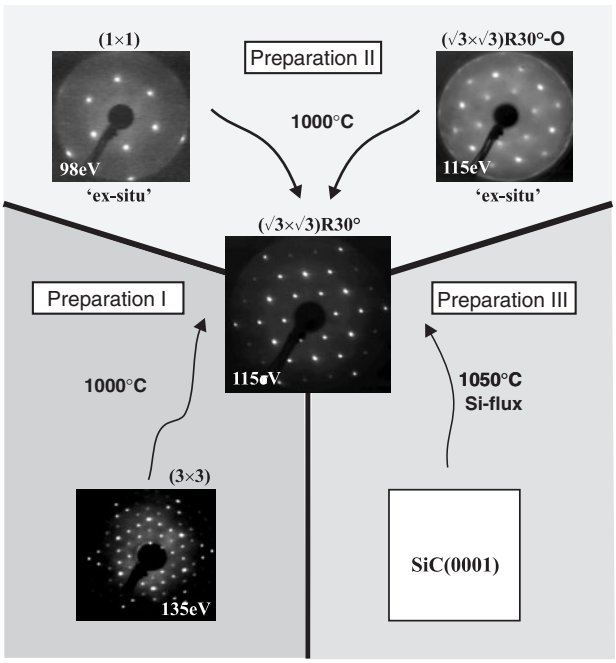

Figure 9. Different preparation procedures of the $(\sqrt{3} \times \sqrt{3})$R30° phase.

of figure 10 and shown in line 4 of table 1. Within the limits of error, there are no S3-stacked domains. Instead, there is a clear dominance of S2-stacking. The presence of oxygen (originating from the silicate phase) seems possibly to inhibit the formation of S3-stacking—a suspicion supported by similar findings after oxygen adsorption/desorption experiments [8]. To further demonstrate the stacking flexibility during formation of the $(\sqrt{3} \times \sqrt{3})$R30° phase, we note that by preparation via a further procedure, namely (as displayed in panel III of figure 9) via annealing *any* surface phase at some temperature in the range 1050–1100 °C under simultaneous Si flux ($\approx 1/4$ ML min^{-1}), leads again to spectral modifications (spectrum III in figure 10) and to a substantial weight of S3-stacking (line 5 in table 1). Stacking rearrangements have also been found on annealing H-terminated 6H samples [34].

It seems that preparation of the $(\sqrt{3} \times \sqrt{3})$R30° phase under Si-rich conditions favours the change to S3-stacking, i.e. the tendency towards cubic stacking, while the presence of oxygen inhibits it. The stacking rearrangement is certainly facilitated by the cubic stacking being energetically preferred [35, 36]. Yet it is accompanied by a substantial reordering on the surface, as is visible in the STM [2, 26, 27] and as is also apparent from the accompanying development of the LEED patterns, as visualized in figure 11. There are a number of intermediate structures and complex structural mixtures that are indicative of the spatially inhomogeneous phase transformation. In the final state that is reached, however, the structure can be rather homogeneous, with a single type of surface stacking predominating. With the latter being almost purely of S3-type, further *cubic* crystal growth may be realized. This bears the potential for the formation of band-gap heterojunctions with sharp and rather defect- and stress-free interfaces.

5. Epitaxial silicate phases

As mentioned in the introduction, the formation of a largely defect-free insulating oxide on SiC to be used, for example, in MOSFETs is problematic. Though SiO_2 can, in principle,

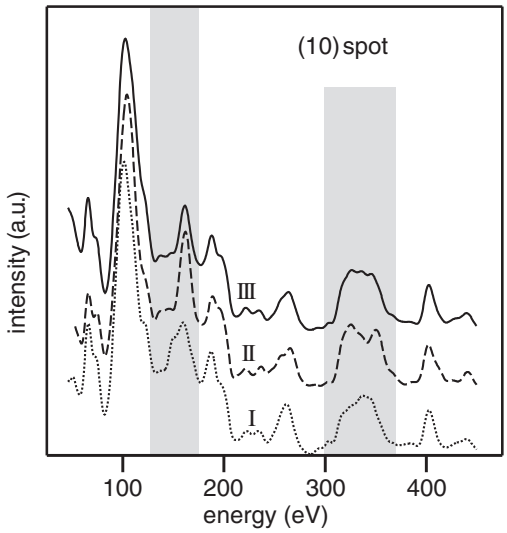

Figure 10. LEED spectra for differently prepared $(\sqrt{3} \times \sqrt{3})$R30° reconstructions of 4H-SiC(0001) (see figure 9) for a selected beam. Most of the changes are observed in the energy ranges indicated by shaded areas.

be arranged on SiC(0001) with just a small misfit (of the order of 5% in a $(\sqrt{3} \times \sqrt{3})$R30° superstructure), its thermal formation with a certain film depth requires the removal of the carbon atoms in many layers (e.g. via CO_2 production), which has been shown to lead to a substantial amount of defects [1]. Therefore, the oxidation behaviour of various surface phases of SiC(0001), in particular silicon-rich surface phases, has recently been the subject of intense investigations (for a compact review, see [37]). Fortunately, however, a defect-free silicate-type epitaxial transition state to SiO_2 can be formed on both the (0001) and $(000\bar{1})$ terminations of hexagonal SiC. This is by *ex situ* preparation of 4H as well as 6H samples, whereby—following some sacrificial oxidation and treatment in HF—the surfaces are etched in a hydrogen flow at elevated temperatures or by a hydrogen plasma. In these treatments, when the simultaneous presence of even tiny amounts of oxygen is not excluded, they lead to a new state of the surface, characterized by a superstructure, again of $(\sqrt{3} \times \sqrt{3})$R30° symmetry [38, 39]. Yet the diffraction intensities are dramatically different from the above-described phase, as shown for a selected beam in the upper two curves of figure 12, indicative for very different structures. So, in order to avoid confusion with the above-described phase of the same symmetry, we use the term $(\sqrt{3} \times \sqrt{3})$R30°-$SiO_x$ for this phase. The reader should also note that the spectra for the (0001) and $(000\bar{1})$ orientations are also very different (the lower two curves of figure 12).

The quantitative analyses of the LEED spectra for the $(\sqrt{3} \times \sqrt{3})$R30°-$SiO_x$ phases on the two surface terminations [38, 39] reveal the structural models shown in figure 13. In each case the top layer is a silicate-like Si–O double layer. Its Si–O elements are in a honeycomb-like arrangement (panel (a)), in the centre of which there is a silicon atom uncoordinated to intralayer oxygen atoms. In the case of the (0001) termination (figures 13(a) and (b)) the silicate layer is attached to the substrate via additional, linear Si–O–Si bonds, while for the $(000\bar{1})$ termination there is direct bonding to the top substrate C atoms (figure 13(c)). As a consequence, the stoichiometry on the (0001) orientation is Si_2O_5, while that on $(000\bar{1})$ is Si_2O_3. Substrate Si or C atoms that were left under-coordinated in these models were found to be saturated by hydrogen [40].

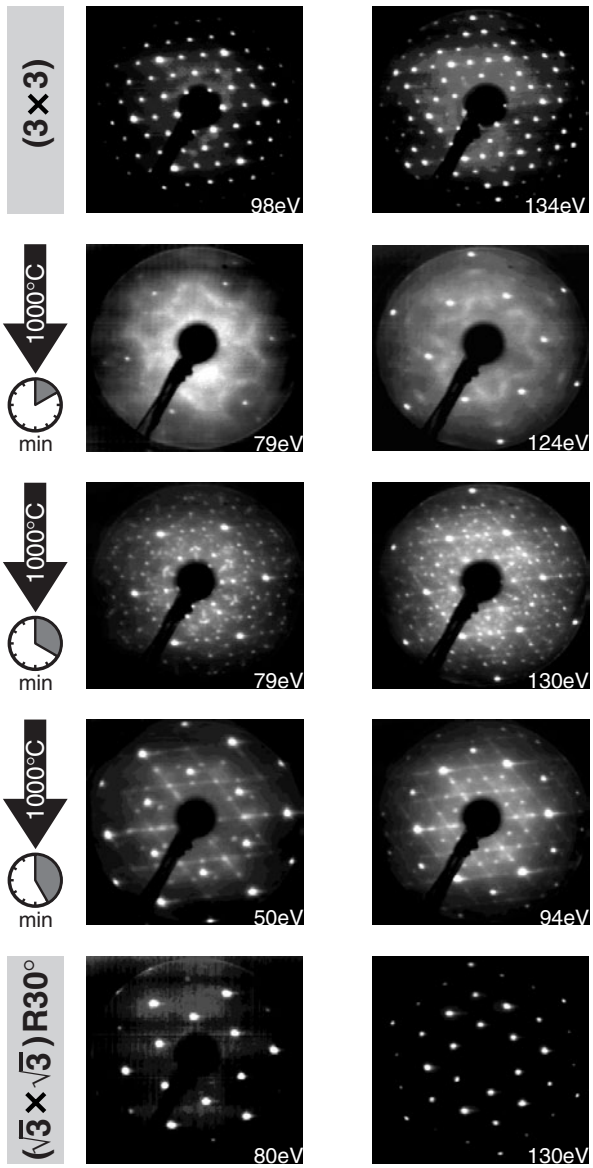

Figure 11. The structural transition from the (3×3) phase to the $(\sqrt{3} \times \sqrt{3})$R30° phase by surface annealing, followed by LEED for a 6H-SiC(0001) surface.

Again, structural parameters and bi-layer stacking for the two surfaces were determined by quantitative LEED [19, 38, 39]. Interestingly, the weight of domains with different stacking termination is quite different for the two orientations: for the 6H sample in the $(000\bar{1})$ orientation, the S1 and S2 terminations dominate (S1:S2:S3 = 45:40:15%); for the 4H-SiC(0001) sample the S1 domain is largely suppressed (S1:S2 = 15:85%). The structural parameters vary slightly with the stacking termination on the surface. The parameter values displayed in figures 13(b), and (c) are averages with respect to all termination domains. They compare favourably with results from DFT calculations [41] and allow the calculation of the

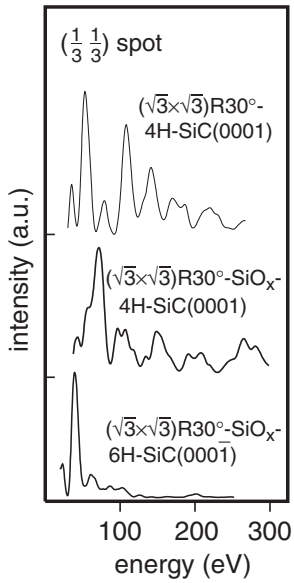

Figure 12. A comparison of spectra for the structural phases $(\sqrt{3} \times \sqrt{3})$R30° and $(\sqrt{3} \times \sqrt{3})$R30°-$SiO_x$, prepared *in situ* and *ex situ*, respectively.

Si–O bond lengths and Si–O–Si bond angles. Within the Si–O double layer, the bond length is 1.61 Å for the silicate on SiC(0001) and 1.64 Å for that on SiC(000$\bar{1}$); the bond angles are 146° and 141°, respectively. These values are very close to that of α-quartz, which are 1.61 Å and 144°. As a consequence, there would be only very little stress at the interface if a thicker film of SiO_2 were grown on the $(\sqrt{3} \times \sqrt{3})$R30°-$SiO_x$ superstructure. Yet for this growth the described Si–O double layer must alter to allow for the three sublayers of SiO_2, i.e. every second Si atom should switch its position, as indicated schematically in figure 14. Simultaneously, of course, the dangling bonds that were additionally introduced at substrate atoms must be saturated. If this could be realized experimentally, oxide films of very low defect density could be grown, suitable for device applications.

6. Summary

In this paper the focus was on a subset of the numerous surface reconstructions of SiC(0001) and SiC(000$\bar{1}$). The reconstructions develop because the bulk truncated surface is rather unfavourable, due to the presence of dangling bonds. As we have seen, the type of reconstruction eventually assumed by the surface depends heavily on the temperature and chemical surrounding that is offered to the surface. Sometimes, details of the preparation are so influential that it is hard to control them to the extent that the production of a certain phase that is wanted can be guaranteed. Nevertheless, it is possible to reliably prepare surface phases that can be functional for an application, in particular for the formation of semiconductor devices based on SiC.

So, the (3×3) reconstruction of 4H- and 6H-SiC(0001) (and also of SiC(111)) is highly passivated, so that atoms arriving for crystal growth can easily diffuse on the surface. Accordingly, they can reach surface steps where they can be built in, and hence crystallographically copy the underlying polytype. Through this step-flow mechanism, the

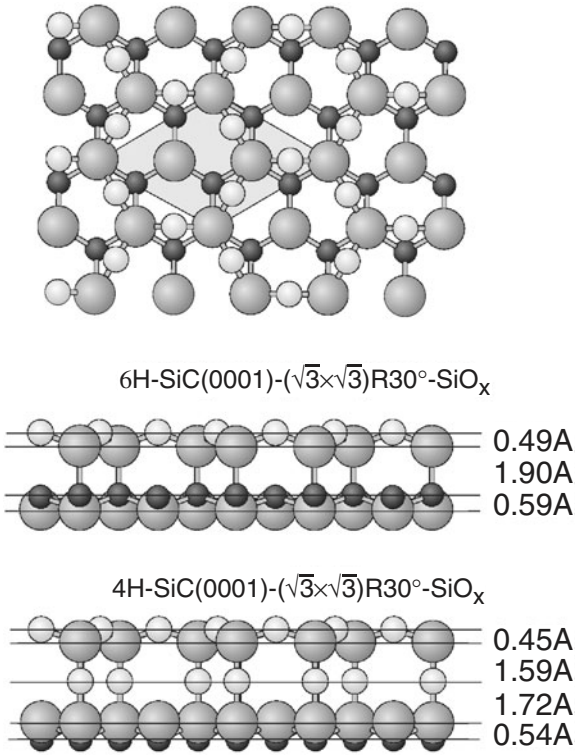

Figure 13. Side-view ball models for the $(\sqrt{3} \times \sqrt{3})$R30°-$SiO_x$ phases of the (0001)- and $(000\bar{1})$-oriented surfaces of 4H- and 6H-SiC, respectively.

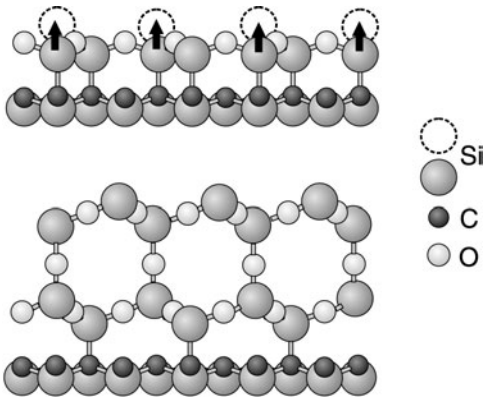

Figure 14. The possible transition of the silicate phase (figure 13(c)) to allow for the growth of a SiO_2 film.

growth of a certain polytype (i.e. single-crystal growth) can be stabilized, which is essential for the use of the material in devices. On the other hand, through the preparation of the $(\sqrt{3} \times \sqrt{3})$R30° reconstruction, the surface can be made to rearrange in favour of one of several possible surface terminations. In particular, the preparation of the superstructure on 4H-SiC(0001) under Si-rich conditions strongly favours the S3-termination—a termination

not existing on the bulk-like terminated surface of this polytype. This opens the gate for the growth of a 3C crystal on top of the 4H polytype. With the different band gaps of the polytypes given, this is equivalent to the production of a band-gap heterojunction which—in view of the almost identical lattice parameters of the polytypes—should be defect- and almost stress-free. Finally, we have shown that surface reconstructions can be prepared on both the (0001) and $(000\bar{1})$ orientation that are characterized by silicate-like epitaxial adlayers. This offers the defect-free attachment of an insulating silicon oxide film, which is important, once again, for device applications. In conclusion, the rich structural flexibility of SiC surfaces may be exploited for the formation of defect-free interfaces relevant for various applications. Yet we also point out that the use of this potential requires substantial further experimental work.

Acknowledgment

This work was supported by Deutsche Forschungsgemeinschaft (DFG) through SFB 292.

References

[1] Cooper J A Jr 1997 *Phys. Status Solidi* a **162** 305
[2] Starke U, Bernhardt J, Schardt J and Heinz K 1999 *Surf. Rev. Lett.* **6** 1129
[3] Heinz K, Starke U, Bernhardt J and Schardt J 2000 *Appl. Surf. Sci.* **162/163** 9
[4] Heine V, Cheng C and Needs R J 1991 *J. Am. Ceram. Soc.* **74** 2630
[5] Verma R and Krishna P 1966 *Polymorphism and Polytypism in Crystals* (New York: Wiley)
[6] Starke U 1997 *Phys. Status Solidi* b **202** 475
[7] Sieber N, Mantel B F, Seyller T, Ristein J, Ley L, Heller T, Batchelor D R and Schmeisser D 2001 *Appl. Phys. Lett.* **78** 1216
[8] Bernhardt J 2001 *PhD Thesis* Universität Erlangen-Nürnberg
[9] Kaplan R 1989 *Surf. Sci.* **215** 111
[10] Starke U, Schardt J, Bernhardt J, Franke M, Reuter K, Wedler H, Heinz K, Furthmüller K, Käckell P and Bechstedt F 1998 *Phys. Rev. Lett.* **80** 758
[11] Schardt J, Bram Ch, Müller S, Starke U, Heinz K and Müller K 1995 *Surf. Sci.* **337** 232
[12] Ascolani H, Cerda J R, de Andres P L, de Miguel J J, Miranda R and Heinz K 1996 *Surf. Sci.* **345** 320
[13] Starke U, Schardt J and Franke M 1997 *Appl. Phys.* A **65** 578
[14] Schardt J, Bernhardt J, Starke U and Heinz K 2000 *Phys. Rev.* B **62** 10335
[15] Kulakov M A, Henn G and Bellemer B 1996 *Surf. Sci.* **346** 49
[16] Li L and Tsong I S T 1996 *Surf. Sci.* **351** 141
[17] Heinz K, Seubert A and Saldin D K 2001 *J. Phys.: Condens. Matter* **13** 10647
[18] Reuter K, Bernhardt J, Wedler H, Schardt J, Starke U and Heinz K 1997 *Phys. Rev. Lett.* **79** 4818
[19] Schardt J 1999 *PhD Thesis* Universität Erlangen-Nürnberg
[20] Furthmüller J, Käckell P, Bechstedt F, Fissel A, Pfenninghaus K, Schröter B and Richter W 1998 *J. Electron Mater.* **27** 848
[21] Badziag P 1998 *Surf. Sci.* **404** 822
[22] Tanaka S, Kern R S and Davis R F 1994 *Appl. Phys. Lett.* **65** 2851
[23] Fissel A, Schröter B and Richter W 1995 *Appl. Phys. Lett.* **66** 3182
[24] Kimoto T, Itoh A, Matsunami H and Okano T 1997 *J. Appl. Phys.* **81** 3494
[25] Matsunami H and Kimoto T 1997 *Mater. Sci. Eng.* R **20** 125
[26] Starke U, Schardt J, Bernhardt J, Franke M and Heinz K 1999 *Phys. Rev. Lett.* **82** 2107
[27] Starke U, Bernhardt J, Schardt J, Seubert A and Heinz K 2000 *Mater. Sci. Forum* **338–342** 341
[28] Seubert A 2002 *PhD Thesis* Universität Erlangen-Nürnberg
[29] Northrup J E and Neugebauer J 1995 *Phys. Rev.* B **52** R17001
[30] Bechstedt F, Käckell P, Zywietz A, Karch K, Adolph B, Tenelson K and Furthmüller J 1997 *Phys. Status Solidi* b **202** 35
[31] Pollmann J, Krüger P and Sabisch M 1997 *Phys. Status Solidi* b **202** 421
[32] Coati A, Sauvage-Simkin M, Garreau Y, Pinchaux R, Argunova T and Aïd K 1999 *Phys. Rev.* B **59** 12224
[33] Fujino T, Fuse T, Ryu J T, Inudzuka K, Yamazaki Y, Katayama M and Oura K 2000 *Japan. J. Appl. Phys.* **39** 6410

[34] Sieber N, Stark T, Seyller T, Ley L, Zorman C A and Mehregany M 2002 *Appl. Phys. Lett.* **80** 4726
[35] Grossner U, Fissel A, Furthmüller J, Richter W and Bechstedt F 2000 *Mater. Sci. Forum* **353–356** 211
[36] Righi M C, Pignedoli C A, Borghi G, Di Felice R, Bertoni C M and Catellani A 2002 *Phys. Rev.* B **66** 45320
[37] Starke U 2004 *Silicon Carbide* ed W J Choyke, H Matsunami and G Pensl (Berlin: Springer) p 285
[38] Bernhardt J, Schardt J, Starke U and Heinz K 1999 *Appl. Phys. Lett.* **74** 1084
[39] Starke U, Schardt J, Bernhardt J and Heinz K 1999 *J. Vac. Sci. Technol.* A **17** 1688
[40] Sieber N, Hollering M, Ristein J and Ley L 2000 *Mater. Sci. Forum* **338–342** 391
[41] Lu W C, Krüger P and Pollmann J 2000 *Phys. Rev.* B **61** 13737